3. Puetter, R. C. & Yahil, A. in *The Astronomical Data Analysis Software and Systems (ADASS) VIII Conference* (eds Mehringer, D. M., Plante, R. L. & Roberts, D. A.) Vol. 172, 307–316 (Astronomical Society Publications, ASP, San Francisco, 1999).
4. Fernández-Soto, A., Lanzetta, K. M. & Yahil, A. A new catalog of photometric redshifts in the Hubble deep field. *Astrophys. J.* **513,** 34–50 (1999).
5. Holtzman, J. A. *et al.* The photometric performance and calibration of WFPC2. *Publ. Astron. Soc. Pacif.* **107,** 1065–1093 (1995).
6. Schmidt, B. P. *et al.* The high-z supernova search: measuring cosmic deceleration and global curvature of the universe using type Ia supernovae. *Astrophys. J.* **507,** 46–63 (1998).

Correspondence should be addressed to H.-W.C. (e-mail: hchen@ociw.edu).

First-order transition in confined water between high-density liquid and low-density amorphous phases

Kenichiro Koga*, Hideki Tanaka† & X. C. Zeng‡

* *Department of Chemistry, Fukuoka University of Education, Fukuoka 811-4192, Japan*
† *Department of Chemistry, Okayama University, 3-1-1, Tsushima, Okayama 700-8530, Japan*
‡ *Department of Chemistry and Center for Materials & Analysis, University of Nebraska, Lincoln, Nebraska 68588, USA*

Supercooled water and amorphous ice have a rich metastable phase behaviour. In addition to transitions between high- and low-density amorphous solids[1,2], and between high- and low-density liquids[3–8], a fragile-to-strong liquid transition has recently been proposed[9,10], and supported by evidence from the behaviour of deeply supercooled bilayer water confined in hydrophilic slit pores[11]. Here we report evidence from molecular dynamics simulations for another type of first-order phase transition—a liquid-to-bilayer amorphous transition—above the freezing temperature of bulk water at atmospheric pressure. This transition occurs only when water is confined in a hydrophobic slit pore[12–14] with a width of less than one nanometre. On cooling, the confined water, which has an imperfect random hydrogen-bonded network, transforms into a bilayer amorphous phase with a perfect network (owing to the formation of various hydrogen-bonded polygons) but no long-range order. The transition shares some characteristics with those observed in tetrahedrally coordinated substances such as liquid silicon[15,16], liquid carbon[17] and liquid phosphorus[18].

A popular model of water—the TIP4P model—was employed[19] in the molecular dynamics (MD) computer simulation. The melting temperature of the three-dimensional (3D) TIP4P normal ice (I_h) at ambient pressure (0.1 MPa) was recently estimated to be about 237 ± 7 K (ref. 20). We prepared a thin film of TIP4P water by confining the water molecules between two parallel walls fixed in a space. The wall–wall separation was taken to be just enough to accommodate two molecular layers. The water–wall interaction was modelled by a 9-3 Lennard–Jones potential (hydrophobic wall)[13]. The MD simulations were performed under the condition of fixed temperature and fixed lateral pressure (pressure tensor components parallel to the walls), using a modified Nosé–Andersen method. In the first series of MD simulations, a system of 960 molecules (system A) was cooled from 400 K to 210 K in steps and then heated back to 400 K, at a lateral pressure of 0.1 MPa. Three independent MD simulations were carried out with this cooling-and-heating process. In the second series, a system of 240 molecules (system B) was used to examine the phase behaviour at several fixed pressures: 0.1 MPa, 100 MPa, 300 MPa and 1 GPa. At each pressure the temperature was, again, lowered in steps. The MD simulation time ranged from 200 ps to 20 ns, depending on the temperature and pressure of the system. For the sake of structure analysis, configurations of system A at 275, 270 and 210 K were mapped respectively onto the inherent structures[21] by means of the steepest descent method at a fixed volume.

Figure 1 shows the temperature dependence of the potential energies at a fixed pressure of 0.1 MPa. As the system is cooled, the potential energy first gradually decreases and then suddenly drops by about 5.6 kJ mol^{-1} to a lower value at 270 K. This large energy drop within a small temperature range (5 K) is comparable to that (7.0 kJ mol^{-1}, ref. 20) at the freezing transition of TIP4P bulk water and is much larger than that (1.2 kJ mol^{-1} at 200 MPa, ref. 6) at the high-density liquid (HDL) to low-density liquid (LDL) transition in supercooled TIP4P bulk water. In the reversed heating process, the potential energy jumps to a higher value at around 300 K, following the trace of the cooling process. The sharp changes in energy and the large hysteresis appearing in the cooling and heating processes suggest a strong first-order phase transition in the confined water. The temperature dependence of the density of the system also shows that the transition is first-order, as the density initially increases gradually with lowering the temperature but then decreases steeply at the transition temperature (by about 1% at 0.1 MPa and 4% at 300 MPa). Moreover, the diffusion constants calculated before and after the transition (at 275 K and 270 K respectively) differ by four orders of magnitude. The mechanism is also changed at this temperature from a free diffusion to a jump diffusion, which is highly cooperative but involves very few molecules. This order-of-magnitude change in diffusivity is comparable to that of the liquid-to-crystalline ice transition in the 3D TIP4P system (Table 1), as well

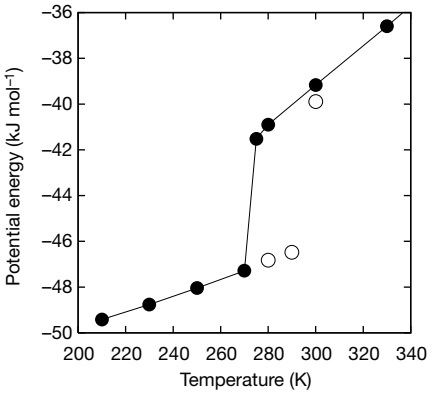

Figure 1 Temperature dependence of the potential energy. The potential energy consists of the water–water intermolecular interactions and the water–wall interactions. Filled and unfilled circles indicate the cooling and heating processes, respectively.

as to that of real water at the liquid-to-crystalline ice transition[22–24]. The drastic change in diffusivity within a small temperature range (5 K) suggests that the confined liquid water transforms into a very viscous 'solid-like' amorphous phase around 270 K, 33 K above the melting temperature of the TIP4P ice at 0.1 MPa. In contrast, only about one order of magnitude is the diffusivity change in TIP4P bulk water within a temperature range (213–233 K at 0.1 MPa and 173–183 K at 200 MPa) of a possible HDL–LDL transition (Table 2).

Shown in Fig. 2a and b are inherent structures of the liquid and the new bilayer amorphous phase, respectively. In the amorphous phase, the two molecular layers are nearly flat; the spatial arrangements of oxygen atoms in both layers are being superimposed on each other (that is, they have a symmetry of reflection). These two features do not show up in the liquid phase. More crucial is the difference in the hydrogen-bond network structure. In the new bilayer amorphous phase, every molecule is hydrogen-bonded with four nearest-neighbour molecules (except for a few defects) so that three neighbours are in the same layer and the fourth one is in the opposite layer. Consequently, the hydrogen-bond network of the amorphous phase is almost perfect. Indeed, the substantial decrease in potential energy as well as the loss of fluidity upon the phase transition can be attributed mainly to the formation of the nearly perfect bilayer hydrogen-bond network. In passing, we point out that the observed liquid-to-bilayer amorphous transition occurs only in the two-layer water system. We have also examined a three-layer water system in a thicker nanopore. No liquid-to-bilayer amorphous transition was seen at 0.1 MPa.

Although the bilayer amorphous phase has a local network structure very similar to that of the bilayer crystalline ice[13], it lacks long-range order in the configuration of oxygen atoms, as shown in the radial distribution function (Fig. 2d). There is no translational periodicity in the amorphous phase as there is in the liquid phase. Also, there is a significant spread in hydrogen-bond angles in the two-dimensional (2D) network (Fig. 2e). In contrast, the bilayer crystalline ice does have a periodic unit cell as well as three definite bond angles (Fig. 2c and e). The most notable structural difference between the bilayer amorphous and the bilayer crystalline ice is the variation in the shape of the polygonal rings of hydrogen bonds in each layer. Figure 2b shows that there are not only hexagonal rings but also pentagonal and heptagonal rings, and even some octagonal rings. The distribution of the n-membered rings, which was evaluated on the basis of three independent sets of 100 inherent structures, shows that it is 77% hexagonal ($n = 6$), 11% pentagonal ($n = 5$), 11% heptagonal ($n = 7$) and 1% the other rings ($n = 4, 8, 9, 10$). The appearance of a large number of pentagonal and heptagonal rings indicates that these rings are not some types of imperfection but characteristic constituents of the hydrogen-bond network. Also found is a variety of shapes within each group of n-membered rings, compared to the bilayer crystalline ice in which all the hexagonal rings are congruent. These differences in the network structure between the quasi-2D bilayer amorphous and the bilayer crystalline ice are similar to the fundamental differences between the 2D continuous-random network model of a glass and the regular honeycomb network model of a crystal[25].

Existence of the liquid–liquid and/or amorphous–amorphous transition in supercooled bulk water is still controversial[3–5,7,24,26–28]. Here, our simulation directly demonstrates that water, when confined in a hydrophobic nanopore, can exhibit a sharp transition to a bilayer amorphous phase (bilayer polyamorphism) at a temperature above the melting temperature of the 3D TIP4P ice. In contrast, the HDL–LDL liquid–liquid transition in bulk water is, if it exists, below 210 K (refs 5 and 7). Moreover, the bilayer polyamorphic transition shows a marked change in potential energy, density and diffusion constant within a very small temperature range (5 K). These characteristics of first-order transition are similar to those found in covalent tetrahedral substances[29] including liquid silicon[16], carbon[17], and phosphorus[18].

The relation among the quasi-2D, high-density liquid (bilayer HDL), low-density amorphous (bilayer LDA), and crystalline (bilayer ice) phases can be compared with that among three corresponding 3D HDL, LDL, and crystalline ice (I_h) phases (Table 2): (1) the potential energy differs more strongly between the higher-energy liquid phase and the lower-energy amorphous phase than between the lower-energy amorphous phase and the crystalline phase in inherent structure, a behaviour found in both 2D and 3D systems. (2) At the transition, the population of molecules with coordination number other than 4 nearly vanishes in the quasi-2D system, and also decreases substantially in the 3D system.

Table 2 Analogies between the quasi-2D and 3D systems

	Potential energy* (kJ mol^{-1})		Four-hydrogen-bond species† (%)		Six-membered rings‡ (%)	
Phase	Q2D	3D	Q2D	3D	Q2D	3D
HDL	–47.6	–53.5	73.1	80.2	35.4	46.0
LDL§	–51.9	–55.0	99.7	92.2	76.7	62.2
Crystalline	–53.0	–55.9	100.0	100.0	100.0	100.0

Q2D, quasi-two-dimensional; HDL, high-density liquid; LDL, low-density liquid; LDA, low-density amorphous.
* Average potential energy of inherent structures.
† Average fraction of molecules having four hydrogen-bonding neighbours.
‡ Average number of six-membered rings normalized by the number in a corresponding crystal.
§ Bilayer LDA in the case of the quasi-2D system.

Table 1 Diffusion constants for the TIP4P water in the quasi-2D and 3D systems (in cm^2 s^{-1})

Quasi-2D system

Hydrophobic pore*	Hydrophilic pore†	Hydrophobic pore, larger width‡
275K: 1.3×10^{-5} 270K: 3.0×10^{-9} 250K: 7.9×10^{-11}	250K: 5.0×10^{-7}	250K: 6.2×10^{-6}

3D system

Supercooled (0.1 MPa)	Supercooled (200 MPa)	Ice	Supercooled (exp.)§	Ice (exp.)‖
233K: 2×10^{-6} 213K: 9×10^{-8} 193K: 6×10^{-8}	193K: 3.0×10^{-7} 183K: 1.4×10^{-7} 173K: 9×10^{-9}	240K: 3×10^{-10} 230K: 0¶	263.7K 7.0×10^{-6} 250K: 3.4×10^{-6}	252K: 1.0×10^{-9} 242K: 7.7×10^{-10}

* The system of interest.
† A reference system of water confined in a model hydrophilic slit pore.
‡ Another reference system with a slit width 1.5 times wider than that of the system of interest.
§ Ref. 22.
‖ Ref. 23.
¶ Less than 10^{-11}.

(3) In both 2D and 3D systems, the number of six-membered rings in the hydrogen-bond network differs considerably among the three phases. (4) The diffusion constant changes by at least four orders of magnitude from liquid to the crystalline ice phase or to the bilayer LDA phase (Table 1).

We also examined the phase behaviour of the confined water in a wide range of pressure and temperature with system B. We found that the higher the pressure the lower the transition temperature (265 K at 100 MPa, and 260 K at 300 MPa). This behaviour is consistent with a negative change in entropy ($\Delta S < 0$) and a positive change in volume ($\Delta V > 0$) at the liquid-to-bilayer amorphous phase transition. Moreover, the same transition was observed around 500 MPa in a decompressing process from 1 GPa to 300 MPa at a fixed temperature of 250 K. However, the transition was not observed beyond a high pressure of 1 GPa and above 190 K. The expansion ($\Delta V > 0$) at the liquid-to-bilayer amorphous transition is analogous to that at the bulk water-to-ice freezing transition.

We note that our finding of the first-order liquid-to-bilayer amorphous transition is based on the TIP4P model of water. Confirmation of this finding must await experiments. Recently, Bergman and Swenson[11] studied bilayer water confined in hydrophilic nanopores using broad-band dielectric spectroscopy. They found that about half of the water molecules form a hydrogen bond to one of the wall surfaces and they also found evidence to suggest a fragile-to-strong liquid transition in deeply supercooled water[10]. We have performed a preliminary simulation of bilayer water confined in a model hydrophilic pore. The bilayer HDL to LDA transition was not seen within the timescale of the simulation. The diffusion constant calculated at 250 K is similar to that of bulk liquid water, that is, four orders of magnitude higher than that of the bilayer amorphous phase. In the hydrophobic pores, on the other hand, water molecules do not form hydrogen bonds to the wall surfaces and the bilayer HDL to LDA transition occurs. The question is why such a transition happens only in the hydrophobic nanopore. One explanation may be that when the two-layer water is confined in the

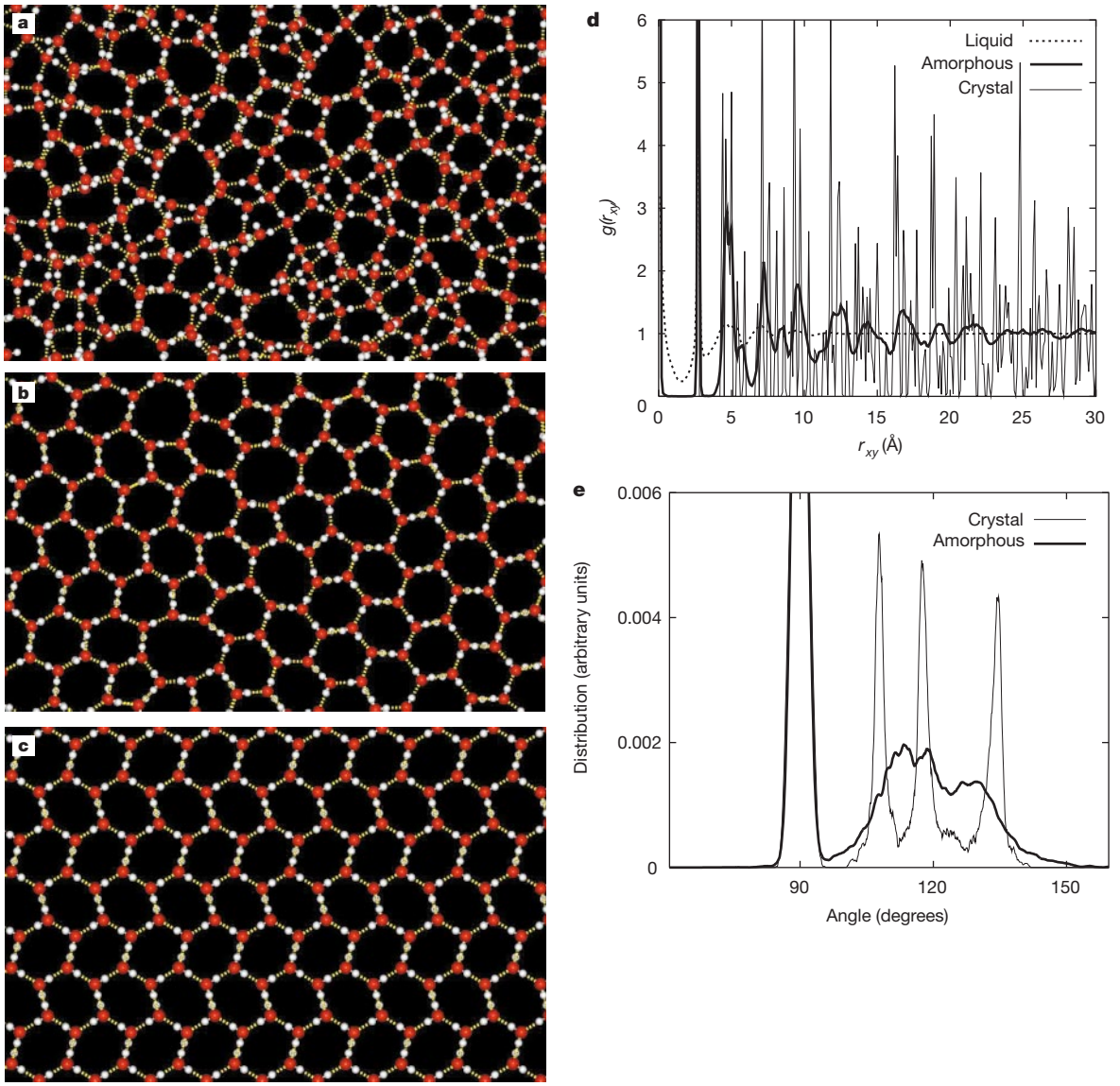

Figure 2 Structure of the confined two-layer water in liquid, amorphous, and crystalline ice phases. **a**, Liquid. **b**, Amorphous. **c**, Crystalline ice. These are top views, showing in-plane (2D) molecular configurations and hydrogen-bond networks. Red and white spheres are oxygen and hydrogen atoms, respectively. Yellow dotted lines indicate the hydrogen bonds. In **b** and **c**, the in-plane 3-connected hydrogen-bond network of one layer is completely superimposed on that of the other layer and the fourth vertical hydrogen bonds connecting two layers are hidden. **d**, Radial distribution function of oxygen atoms. Distance r_{xy} is the distance in a plane parallel to the walls. **e**, Distribution of the hydrogen-bond angles.

hydrophobic nanopore, the geometrical confinement forces the water molecules to form a perfect (coordination number $z = 4$) 2D bilayer hydrogen-bond network even in a topologically disordered structure. However, in the 3D supercooled water the coordination number has a distribution of z-values (3% for $z = 3$ and 2% for $z = 5$) even after the transition to the lower-energy LDL phase[30] (before transition, 11% for $z = 3$ and 5% for $z = 5$). As a result, the LDL phase of 3D supercooled water (below 180 K) has a higher mobility than the bilayer LDA phase, even when the former is at much lower temperatures. Indeed, the diffusion constant of 3D LDL at 173 K (the deeply supercooled region) is still two orders of magnitude higher than that of bilayer LDA at 250 K. □

Received 31 March; accepted 10 October 2000.

1. Mishima, O., Calvert, L. D. & Whalley, E. 'Melting' ice I at 77 K and 10 kbar: a new method of making amorphous solids. *Nature* **310,** 393–394 (1984).
2. Mishima, O., Calvert, L. D. & Whalley, E. An apparently first-order transition between two amorphous phases of ice induced by pressure. *Nature* **314,** 76–78 (1985).
3. Poole, P. H., Sciortino, F., Essmann, U. & Stanley, H. E. Phase behaviour of metastable water. *Nature* **360,** 324–328 (1992).
4. Stanley, H. E. *et al.* Is there a second critical point in liquid water? *Physica A* **205,** 122–139 (1994).
5. Tanaka, H. A self-consistent phase diagram for supercooled water. *Nature* **380,** 328–330 (1996).
6. Tanaka, H. Phase behaviors of supercooled water: Reconciling a critical point of amorphous ices with spinodal instability. *J. Chem. Phys.* **105,** 5099–5111 (1996).
7. Sciortino, F., Poole, P. H., Essmann, U. & Stanley, H. E. Line of compressibility maxima in the phase diagram of supercooled water. *Phys. Rev. E* **55,** 727–737 (1997).
8. Mishima, O. & Stanley, H. E. The relationship between liquid, supercooled and glassy water. *Nature* **396,** 329–335 (1998).
9. Angell, C. A. Water-II is a strong liquid. *J. Phys. Chem.* **97,** 6339–6341 (1993).
10. Ito, K., Moynihan, C. T. & Angell, C. A. Thermodynamic fragility in liquids and a fragile-to-strong liquid transition in water. *Nature* **398,** 492–495 (1999).
11. Bergman, R. & Swenson, J. Dynamics of supercooled water in confined geometry. *Nature* **403,** 283–286 (2000).
12. Bellissent-Funel, M.-C., Chen, S. H. & Zanotti, J. M. X-ray and neutron scattering studies of the structure of water at a hydrophobic surface. *J. Chem. Phys.* **104,** 10023–10029 (1996).
13. Koga, K., Zeng, X. C. & Tanaka, H. Freezing of confined water: a bilayer ice phase in hydrophobic nanopores. *Phys. Rev. Lett.* **79,** 5262–5265 (1997).
14. Meyer, M. & Stanley, H. E. Liquid-liquid phase transition in confined water: A Monte Carlo study. *J. Phys. Chem. B* **103,** 9728–9730 (1999).
15. Thompson, M. O. *et al.* Melting temperature and explosive crystallization of amorphous silicon during pulsed laser irradiation. *Phys. Rev. Lett.* **52,** 2360–2363 (1984).
16. Angell, C. A., Borick, S. S. & Grabow, M. H. Glass transitions and first order liquid-metal-to-semiconductor transitions in 4-5-6 covalent systems. *J. Non-Cryst. Solids* **205,** 463–471 (1996).
17. Glosli, J. N. & Ree, F. H. Liquid-liquid phase transformation in carbon. *Phys. Rev. Lett.* **82,** 4659–4662 (1999).
18. Katayama, Y. *et al.* A first-order liquid–liquid phase transition in phosphorus. *Nature* **403,** 170–173 (2000).
19. Jorgensen, W. L., Chandrasekhar, J., Madura, J. D., Impey, R. W. & Klein, M. L. Comparison of simple potential functions for simulating liquid water. *J. Chem. Phys.* **79,** 926–935 (1983).
20. Gao, G. T., Zeng, X. C. & Tanaka, H. The melting temperature of proton-disordered hexagonal ice: A computer simulation of TIP4P model of water. *J. Chem. Phys.* **112,** 8534–8538 (2000).
21. Stillinger, F. H. A topographic view of supercooled liquids and glass formation. *Science* **267,** 1935–1939 (1995).
22. Gillen, K. T., Douglass, D. C. & Hoch, M. J. R. Self-diffusion in liquid water to −31°. *J. Chem. Phys.* **57,** 5117–5119 (1972).
23. Goto, K., Hondoh, T. & Higashi, A. Determination of diffusion coefficients of self-interstitials in ice with a new method of observing climb of dislocations by X-ray topography. *Jpn J. Appl. Phys.* **25,** 351–357 (1986).
24. Smith, R. S. & Kay, B. D. The existence of supercooled water at 150 K. *Nature* **403,** 283–296 (1999).
25. Zallen, R. in *The Physics of Amorphous Solids* 63–67 (Wiley, New York, 1998).
26. Tse, J. S. *et al.* The mechanisms for pressure-induced amorphization of ice Ih. *Nature* **400,** 647–649 (1999).
27. Soper, A. K. & Ricci, M. A. Structures of high-density and low-density water. *Phys. Rev. Lett.* **84,** 2881–2884 (2000).
28. Scala, A., Starr, F. W., La Nave, E., Sciortino, F. & Stanley, H. E. Configurational entropy and diffusivity of supercooled water. *Nature* **406,** 166–169 (2000).
29. Angell, C. A., Bressel, R. D., Hemmati, M., Sare, E. J. & Tucker, J. C. Water and its anomalies in perspective: tetrahedral liquids with and without liquid-liquid phase transitions. *Phys. Chem. Chem. Phys.* **2,** 1559–1566 (2000).
30. Tanaka, H. Fluctuation of local order and connectivity of water molecules in two phases of supercooled water. *Phys. Rev. Lett.* **80,** 113–116 (1998).

Acknowledgements

K.K. and H.T. are supported by the Japan Society for the Promotion of Science (JSPS), the Japan Ministry of Education, and the Institute for Molecular Science (IMS). X.C.Z. is supported by the US NSF and Office of Naval Research (ONR), and by a JSPS fellowship.

Correspondence and requests for materials should be addressed to K.K. (e-mail: kenkoga@fukuoka-edu.ac.jp).

Changes in deep-water formation during the Younger Dryas event inferred from ^{10}Be and ^{14}C records

Raimund Muscheler*, Jürg Beer *, Gerhard Wagner* & Robert C. Finkel†

** Department of Surface Waters, EAWAG, CH-8600, Dübendorf, Switzerland*
† Center for Accelerator Mass Spectrometry, and Geosciences and Environmental Technology Division, Lawrence Livermore National Laboratory, Livermore, California 94550, USA

Variations in atmospheric radiocarbon (^{14}C) concentrations can be attributed either to changes in the carbon cycle[1]—through the rate of radiocarbon removal from the atmosphere—or to variations in the production rate of ^{14}C due to changes in solar activity or the Earth's magnetic field[2]. The production rates of ^{10}Be and ^{14}C vary in the same way, but whereas atmospheric radiocarbon concentrations are additionally affected by the carbon cycle, ^{10}Be concentrations reflect production rates more directly. A record of the ^{10}Be production-rate variations can therefore be used to separate the two influences—production rates and the carbon cycle—on radiocarbon concentrations. Here we present such an analysis of the large fluctuations in atmospheric ^{14}C concentrations, of unclear origin[3], that occurred during the Younger Dryas cold period[6]. We use the ^{10}Be record from the GISP2 ice core[5] to model past production rates of radionuclides, and find that the largest part of the fluctuations in atmospheric radiocarbon concentrations can be attributed to variations in production rate. The residual difference between measured ^{14}C concentrations and those modelled using the ^{10}Be record can be explained with an additional change in the carbon cycle, most probably in the amount of deep-water formation.

The causes of the variation in Δ^{14}C during the Younger Dryas climate event are the subject of current debate[3,4,6–9]. Δ^{14}C is used as a measure of the atmospheric radiocarbon concentration, and is defined as the per mil deviation from the National Institute of Standards and Technology ^{14}C standard after correction for decay and fractionation[10]. During the Younger Dryas, Δ^{14}C exhibits a rapid increase followed by a gradual decrease. These changes have been discussed in the context of changes in oceanic deep-water formation[4], but coupled ocean–climate models were not able to reproduce all aspects of the observed changes in Δ^{14}C (ref. 9). Using the reconstructed atmospheric ^{10}Be concentration as a proxy for solar activity in the early Holocene epoch, Goslar *et al.*[3] claimed that it is possible to explain the Δ^{14}C during the Younger Dryas even without assuming changes in the deep-water formation. However, for a quantitative determination of the relative contributions of ocean circulation (or other effects related to the carbon cycle) and production-rate changes, a detailed knowledge of the ^{14}C production rate is crucial, because this rate has a large influence on the variations in atmospheric radiocarbon content[1].

Measurements of cosmogenic ^{10}Be in ice cores can be used to provide the necessary information on the ^{14}C production rate[11]. ^{10}Be and ^{14}C are produced by the interaction of cosmic-ray particles with nitrogen and oxygen in the atmosphere. Recent production-rate calculations[12] allow us to determine the ^{14}C production rate, if the ^{10}Be production rate is known. To compare ^{10}Be and ^{14}C records it is necessary to take into account their different geochemical behaviour. ^{10}Be becomes attached to aerosols and is removed from the atmosphere after a mean residence time of 1–2 yr (ref. 13). By contrast, after its production ^{14}C becomes oxidized to $^{14}CO_2$ (ref. 2) and hence is involved in exchange processes between the atmosphere, biosphere and ocean as a constituent of the carbon